

Evaluation of Recycled Aggregates and Bitumen Stabilized Material Cracking Resistance Using Aggregate Imaging and Semi-Circular Bending Tests

Laurence Bridgemohan¹, Lee P Leon^{2,*}, Trevor Townsend¹, Tamika Sinanan²

¹Department of Civil and Environmental Engineering, University of the West Indies, Trinidad and Tobago

²Eastern Regional Health Authority, Ministry of Health, Trinidad and Tobago

Received October 4, 2024; Revised December 4, 2024; Accepted December 24, 2024

Cite This Paper in the Following Citation Styles

(a): [1] Laurence Bridgemohan, Lee P Leon, Trevor Townsend, Tamika Sinanan, "Evaluation of Recycled Aggregates and Bitumen Stabilized Material Cracking Resistance Using Aggregate Imaging and Semi-Circular Bending Tests," *Civil Engineering and Architecture*, Vol. 13, No. 1, pp. 691 - 706, 2025. DOI: 10.13189/cea.2025.130144.

(b): Laurence Bridgemohan, Lee P Leon, Trevor Townsend, Tamika Sinanan (2025). *Evaluation of Recycled Aggregates and Bitumen Stabilized Material Cracking Resistance Using Aggregate Imaging and Semi-Circular Bending Tests*. *Civil Engineering and Architecture*, 13(1), 691 - 706. DOI: 10.13189/cea.2025.130144.

Copyright©2025 by authors, all rights reserved. Authors agree that this article remains permanently open access under the terms of the Creative Commons Attribution License 4.0 International License

Abstract A sustainable pavement engineering approach that makes more use of recycled aggregates is bitumen stabilization technology. Accurately characterizing the parent materials and behavioral traits of bitumen stabilized material (BSM) is now more and more crucial for its performance. The study's two objectives are to: (1) use the aggregate imaging system (AIMS) to examine the morphological characteristics of crushed stone, recycled concrete aggregate (RCA), and recycled asphalt pavement (RAP) both before and after abrasion; and (2) determine whether the Semi-Circular Bend (SCB) test is a suitable tool for assessing BSM fracture. The recycled coarse aggregate fractions were found to be more angular than the natural crushed stones. The most spherical aggregate was found to be RAP. The study also highlighted the SCB test and showed that the SCB test is a valid technique for evaluating BSM fracture within specified methodological limitations. The amount of time between sample preparation and testing has a significant impact on test results. Furthermore, similar to other bituminous pavement materials, the type of bituminous materials, notch depths, and sample sizes all have a major impact on the fracture energy and toughness index. The study's findings show that BSM with optimized recycled material delivers adequate fracture resistance when compared to conventional materials. The potential for the eco-friendly, sustainable repurposing of building and demolition waste

materials as pavement layer aggregates can improve waste management while safeguarding the environment and natural resources.

Keywords Bitumen Stabilized Material, Recycled Aggregate, AIMS, SCB Test, Pavements, Sustainability

1. Introduction

Exploration and characterization of fracture behavior of Bitumen Stabilized Material (BSM) mixtures are important for improved pavement design. Additionally, an increased demand for improved pavement design and rehabilitation technologies has accompanied an observed rise in global economic pressure, climate change and environmental awareness. As a result of this there has been heightened consideration towards techniques involving the use of recycled materials [1]. A feasible sustainable alternative aggregate for pavement applications is believed to be derived from recycled asphalt pavement and recycled concrete. The benefits of using stabilized material in the base layer or sub-layer for road construction are that it leads to an economical, more durable and sustainable pavement. Bitumen stabilization technology offers a sustainable pavement alternative in addition to enhancing

the availability of quarry aggregate resources and recycled pavement materials. Stress-dependent materials are one method of characterizing BSM. They are pavement materials that have been treated with either bitumen emulsion or foamed bitumen. Parent materials in BSMs are often granular materials, reclaimed asphalt (RA) and previously cement stabilized materials. Notably, although they exist as parent material in BSMs, reclaimed asphalt materials and granular aggregate materials possess different characteristics to BSMs. Thus, the application of the BSM technology is crucial to define the parent materials, usually chosen for the stabilization procedure.

Theoretical descriptions indicate that bitumen-stabilized materials possess a microstructure of three phases: (1) an uncoated mineral mastic phase, (2) an uncoated bitumen mastic phase that connects the skeleton at contact points, and (3) an uncoated aggregate skeleton phase [2]. Similar to granular materials, the uncoated coarse aggregate skeleton promotes inter-particle friction. Bituminous mastic production and enhanced cohesion are mostly dependent on the finer fractions. These highlight how crucial aggregate compatibility is for fine particle coating and granular interlock, which lead to contact bonding. A heightened awareness of the necessity to integrate alternative aggregate sources, such as recycled materials, is accompanied by the increasing emphasis on sustainable pavement methods. In order to facilitate the geometrical characterization of recycled aggregates as parent materials for bitumen stabilization, an analysis of the morphological characteristics of sampled RAP, RCA, and two quarried crushed aggregates with varying mineralogy was conducted.

Aggregates are often categorized as coarse or fine particles according to grain size, each significantly influencing the functional performance of the road surface [3, 4]. Under repetitive loading, aggregate morphology changes due to tire impact and friction, which may result in increased rutting and decreasing strength qualities. Aggregate geometric features such as aggregate shape, angularity, and texture have been recognized as influencing variables in unbound aggregate materials' robust and permanent deformation behavior [5]. It is imperative to assess the morphology of the aggregate in order to optimize the performance of the pavement material layer. Visual inspection methods were initially employed to quantify these features during the execution of early applications of standardized test procedures. Nevertheless, these methods have a number of disadvantages, including a labor-intensive, operator-subjective procedure, poor precision and repeatability, and challenges in reliably detecting angular and cubical aggregates [6]. Advancements in technology have led to the creation of diverse automated imaging analysis systems that can capture photos and evaluate the forms of a broad spectrum of aggregate kinds and dimensions. Masad and Fletcher [7] noted that compared to

the current approaches being employed in the practice, there are several benefits of using the Aggregate Imaging System (AIMS). In particular the analysis methods to measure aggregate shapes are unaffected by grain size and provide a direct method of measurement.

BSMs have properties comparable to uncoated coarse granular aggregates. For materials stabilized with either bitumen emulsion or foamed bitumen, bitumen is preferentially disseminated among the finer particles in the parent material aggregate [8, 9]. A non-continuous localized bonding is the result of the isolated bitumen-rich particulates being mechanically pressed against the aggregate particles surrounding them when BSMs are compacted [8]. In asphaltic concrete, bitumen, which is a continuum, binds all aggregate particles together. Previous research into the fracture behavior of asphaltic concrete mixes has established its significance for pavement material characterization. Because of its simplicity, repeatability, and reliability [10], the SCB test was selected as a good method to investigate the fracture behavior of BSM pavement base layer mixtures in this investigation. Constant-rate monotonic loading is used in the SCB test, and a load-displacement curve is recorded for later analysis [11]. The semi-circular bending Illinois flexibility index (SCB-FI) test is one of the most well-known SCB testing modalities since it may determine how readily asphalt mixes crack [12]. Research using the SCB test technique has demonstrated great results, as evidenced by [13-17].

The study's goals are to: (1) use the aggregate imaging system (AIMS) to examine the morphological characteristics of natural graded crushed stone (GCS), recycled concrete aggregate (RCA), and reclaimed asphalt pavement (RAP) before and after abrasion; and (2) investigate how reliable the Semi-Circular Bend (SCB) test is for assessing BSM fracture. This information has the potential to enhance the current theory of parent material characterization and contribute to the known parent material attributes of these extensively used materials, in addition to expanding the number of applications for recycled materials. Additionally, it will aid in determining whether material characterization techniques for bituminous mixes can be employed to evaluate the degree of distress in a stabilized layer. Furthermore, the environmentally friendly, sustainable repurposing of construction recycled materials as pavement layer aggregates have the potential to improve waste management while simultaneously preserving the environment and natural resources.

2. Materials and Methods

2.1. Aggregate

Reclaimed Asphalt Pavement, andesite, Trinidad northern range blue limestone, and Recycled Concrete Aggregate are the aggregates utilized to study the

morphological features. The coarse particle sizes that were utilized ranged from 4.75 to 25 mm. To be more precise, the andesite aggregates came from St. Lucia, the limestone aggregates from National Quarries Company Limited in Trinidad, the RCA aggregates came from demolition waste at construction sites in Trinidad, and the RAP aggregate came from Danny's Enterprises Limited in Trinidad. To prepare them for more testing, these aggregates were sieved, cleaned, and dried. The RCA and RAP were further crushed and prepared to meet the gradation required for BSM aggregate material grading acceptance.

2.2. BSM Mix Design

For the design of the BSM specimens in this study, Graded Crushed Limestone (GCS) and RAP materials were used. The maximum aggregate particle size used to manufacture the natural and recycled aggregate designed BSM mixture was 37.5 mm with grading meeting recommendation of the TG2 [8]. The GCS-BSM samples were stabilized with 2.4% foamed bitumen and the RAP-BSM samples were stabilized using 2% foamed bitumen and an addition of 1% ordinary Portland cement. This was done in a WLB 10 Foaming Unit. All samples were made using 60/70 penetration grade polymer modified bitumen and mixed in a WLM30 Mixer. Table 1 highlights the physical and design properties of the BSM design with both natural and recycled aggregate.

2.3. SCB Sample Preparation

The Semi-Circular Bend (SCB) test samples were fabricated using a 150 mm diameter mold. The pertinent

mix design was followed to prepare each batched sample. The mixture was subsequently poured into the mould and compressed using a compactor to achieve sample thicknesses of 40mm and 50mm. Additional processing was performed on each cylindrical sample to produce two semi-circle sections. Notches of varied lengths (0 mm, 12.5 mm, and 25 mm) were carved into the cut-side of the semicircular face. A total of 72 samples were prepared for testing.

2.4. Aggregate Imaging System Analysis

The Aggregate Imaging System (AIMS) allows for the reliable and consistent evaluation of aggregate morphological properties [18]. The AIMS utilizes computer-based digital imaging and is capable of determining the morphological characteristics of fine and coarse aggregate particles of sizes ranging between 0.075 mm to 37.5 mm [19]. Figure 1 shows the system, which includes a microscope camera, an aggregate tray, and a back and top illumination system [20]. Aggregates were dried, sieved and separated in bags into particle sizes of 19 mm, 12.5 mm, 9.5 mm. and 4.75 mm. Samples of each size of the aggregates were randomly chosen for particle characteristics measurement using the AIMS device. The AIMS analysis was used before and after the Los Angeles Abrasion test to measure the effects of abrasion on the morphological characteristics of the research aggregates. The AIMS testing was done in accordance with ASTM C802-96 [21] and ASTM C1067 [22]. The shape properties measured are highlighted in Fig. 1. The aggregate particles measured in the AIMS device were all marked for ease of identification after the abrasion test.

Table 1. Properties of the Bitumen Stabilized Material and its designation

Sample Dimensions (mm) and Designation	Notch Depths (mm)	Materials	Stabilizing Agent	Bitumen
150x40x75 RAP-40	0	RAP	2% Foamed Bitumen 1% ordinary Portland cement	60/70 Fine Grade
150x50x75 RAP-50	12.5			
	25			
150x40x75 GCS-40	0	GCS	2.4% Foamed Bitumen 1% ordinary Portland cement	60/70 Fine Grade
150x50x75 GCS-50	12.5			
	25			

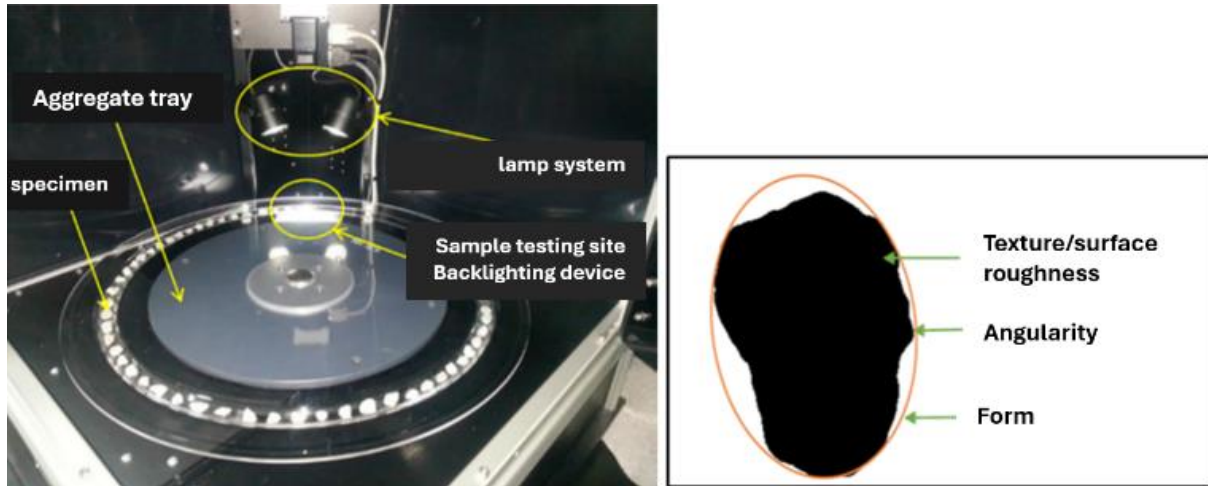


Figure 1. AIMS device and aggregate shape properties

2.5. Los Angeles Abrasion

The Los Angeles abrasion test was conducted in accordance with the ASTM C131 [23]. A five-kilogram sample of aggregate material was placed in the LA abrasion drum, together with 12 steel balls, and rotated for 500 revolutions. To reduce the loss of fine materials, the inside of the drum and the steel balls were meticulously hand-brushed after each turn. Materials that passed through each sieve size were weighed and bagged for subsequent measurement in the AIMS apparatus. This stage was performed to obtain imaging-based quantifications of particle size and shape indices following the LA abrasion runs, and the operation was repeated for each aggregate type. Two LA abrasion tests were performed on each aggregate type, and the average wear percentage was obtained.

2.6. Fracture Properties

The notched specimens were individually inserted into the SCB device [24] using a simply supported, three-point bending setup, as shown in the schematic in Fig. 2. The testing device's maximum span length is 200 mm. The device rollers have a diameter of 25.4 mm and can revolve freely to eliminate friction. The center loading point has a radius of 12.7 mm and can swivel transversely to facilitate more consistent loading across the breadth. The loading rate for SCB testing is following AASHTO TP 124 [25]. The constant displacement rate of 50 mm/minute was swiftly delivered at the halfway, which is located slightly above the notch on the upper surface. In the course of the loading procedure, the mid-span displacement was measured and quantified. While a 10 kN load cell monitored the load that was being delivered, the actuator was responsible for detecting the load-line displacement. As in previous research [26, 27] each SCB test consisted of

three replicates, and the average value was utilized to determine findings.

BSM fracture occurs when available energy exceeds material resistance, which can take many forms, including surface energy or plastic work [28]. The properties calculated from the load-displacement curves (Fig. 2) data are tensile strength, fracture energy and fracture toughness. Tensile Strength as indicated by Equation (1), is the maximum load that the material can support without fracture whilst being stretched, divided by the original cross-sectional area of the material [29]. Fracture energy (G_f) is the quantity of energy required to generate a unit area of a fracture. It is determined by dividing the area under the curve by the ligament area for each sample, as outlined in Equation (2) [30]. The ability of brittle materials to withstand the propagation of faults when subjected to stress is referred to as fracture toughness. This property is based on the concept that the longer a crack is, the less force is necessary to cause the crack to fracture. This was calculated by Equation (3).

$$\sigma = F / 2rt \quad (1)$$

$$G_f = W_f / A_{lig} \quad (2)$$

$$K_{IC} = Y_1 (P/2rt) \sqrt{(\pi a)} \quad (3)$$

$$Y_1 = 4.782 + 1.219(a/r) + 0.063e^{7.045(a/r)} \quad (4)$$

To determine a stress concentration, a notch was placed along each specimen's symmetry axis during the SCB testing procedure [31]. Compared to unnotched specimens, notched SCB specimens exhibited a wider range of fracture toughness [32]. The phase of fracture propagation may be influenced by the non-uniform features of the asphalt mixtures, which result in a variation in the material properties near the notch tip [33]. Therefore, to provide a SCB test technique for BSM in this work, the notched and un-notched SCB tests were selected as an appropriate assessment.

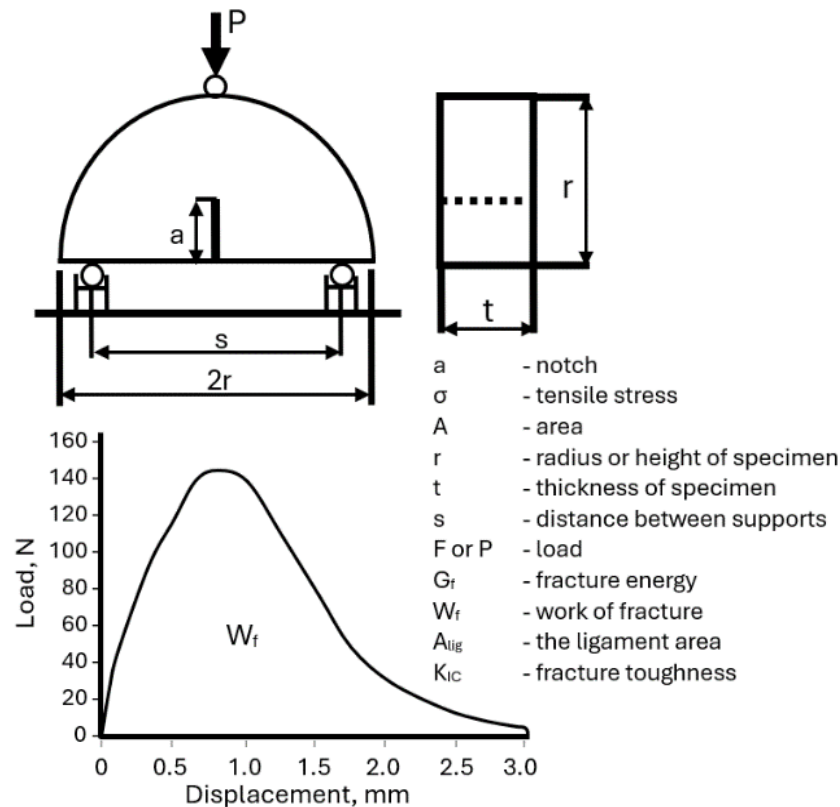


Figure 2. SCB test setup with typical load-displacement curve

3. Results and Discussion

3.1. Abrasion Properties

The geometry of an aggregate in the LA Abrasion test is expected to change due to the interaction with the aggregate and the steel balls during test process. The test results highlighted a clear distinction in the resistance of the aggregates to abrasion which may be due to the variations in the mineral composition and hardness property. For each aggregate, two parallel test sets were run, and the average outcomes are displayed in Fig. 3. The RCA aggregates have the least resistance to abrasion followed by limestone, RAP and andesite respectively. The andesite aggregate has abrasion wear values of less than 20%, thus indicating its ability to withstand impact of traffic loading. Typically, the acceptance criterion for the percentage of LA abrasion wear for use granular aggregate in pavements is <40%.

3.2. Aggregate Morphological Shape Characteristics

Figure 4 shows a comparison of the angularity of four distinct coarse aggregate types (limestone, andesite, RCA, and RAP) both before and after they were put through an abrasion test. These results are consistent with that obtained by [34] with an observed reduction in the angularity for all aggregates after being subjected to abrasion. This development may have been because of

contact between aggregate and the steel spheres, since the angular portions of the aggregate will have been the first to make contact with the steel spheres. Additionally, observed differences in angularity distributions amongst the coarse aggregate particles may be attributed to differences in mineralogy.

Figure 5 highlighted below identifies a 36% decrease in the mean value of angularity for RAP aggregate, with a reduction from 3952 to 2518, and the most significant of the three investigated materials. Additionally, andesite aggregates displayed the least significant angularity reduction of all the tested materials, followed by limestone and RCA. This observation contrasted with the findings of the abrasion test and may have been because of variable mineral compositions of coarse aggregates, which vary from location to location. Owing to its low hardness, the calcite in the limestone, the binder coating in the RAP aggregates, and the mortar in the RCA aggregates were all quickly abraded during the abrasion process. Consequently, the aggregate's edges and corners were easily smoothed, which led to a high abrasion value. Andesite displayed the highest abrasion resistance of any other rock type. Prior to the abrasion test, Figure 5 demonstrated that a greater number of aggregates were in the moderate and high angularity ranges, while a smaller percentage were in the low angularity range. This finding implies that the abrasion test produced a preponderance of aggregates with a low angularity.

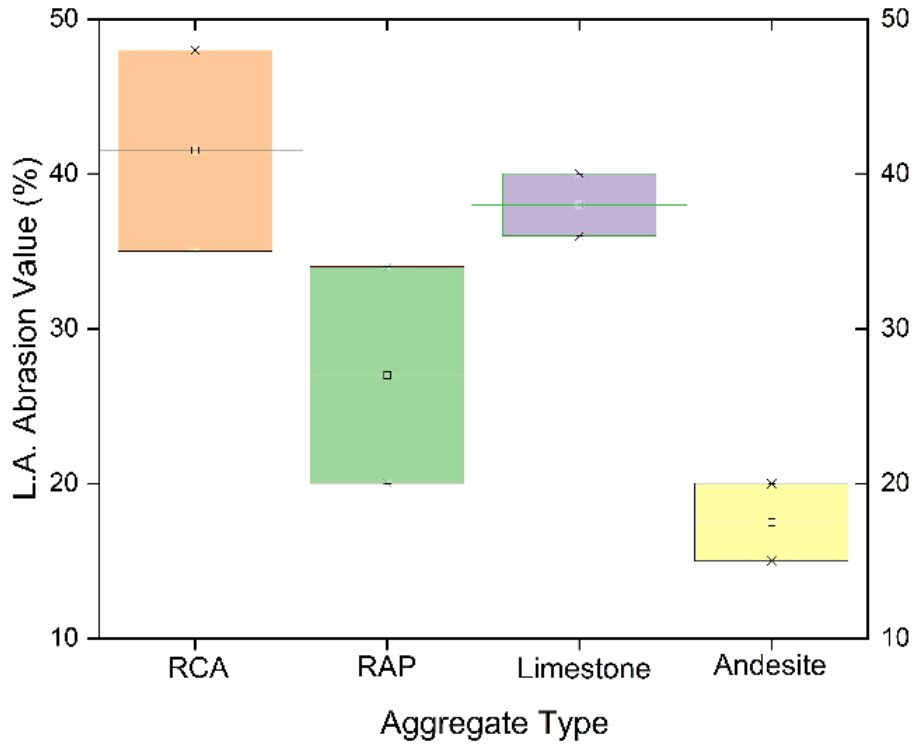


Figure 3. Ranges of aggregate type and their L.A. abrasion wear values

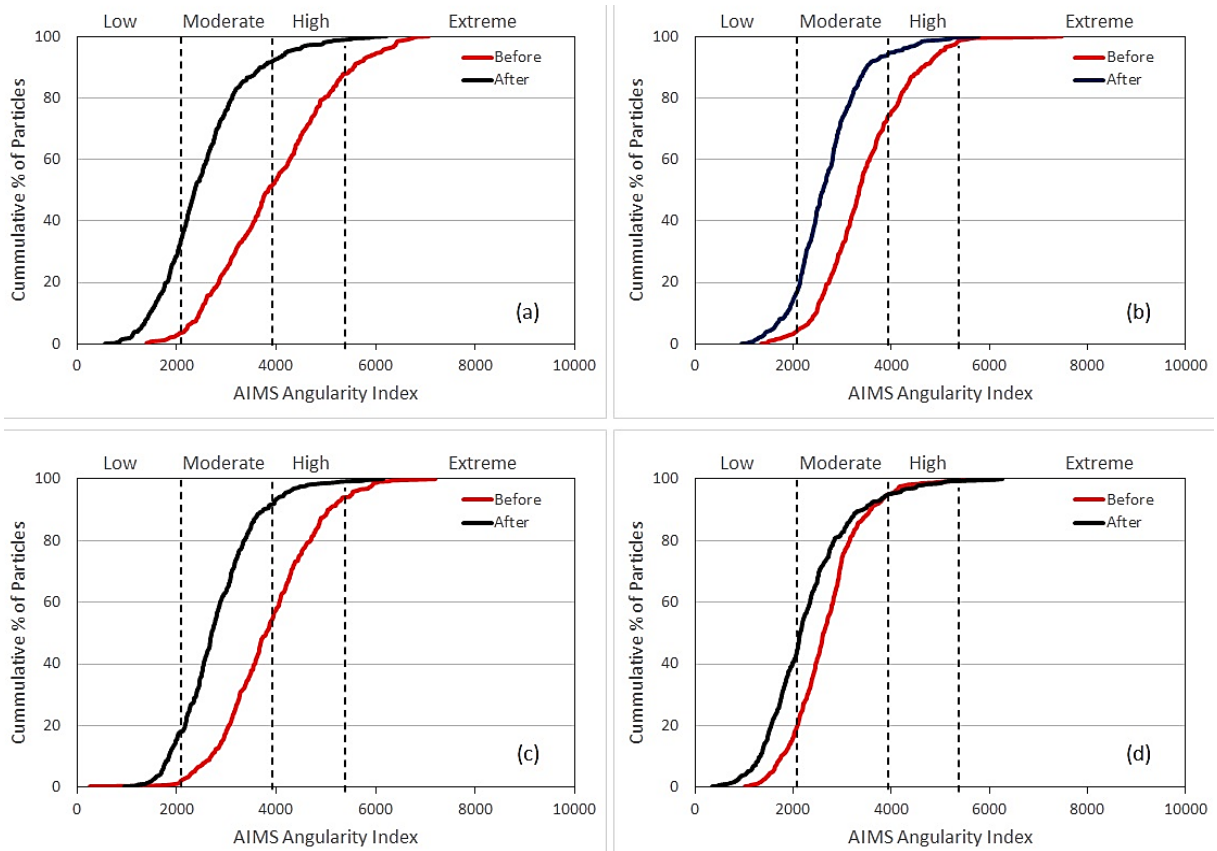


Figure 4. Particle angularity pre- and post-L.A. abrasion wear test (a) crushed Limestone (b) crushed Andesite (c) RAP (d) RCA

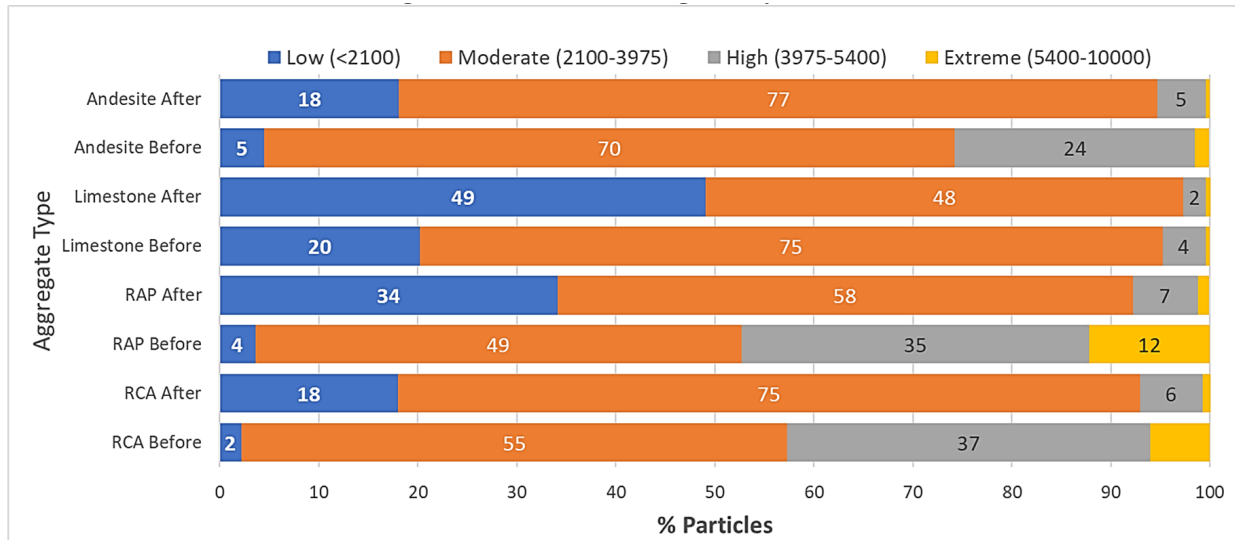


Figure 5. Angularity distribution of aggregates pre- and post-L.A. abrasion wear test

The texture distribution of four distinct coarse aggregate types is shown in Fig. 6 both before and after they undergo an abrasion test. The surface texture of coarse aggregates becomes finer as a result of abrasion, which is analogous to the reduction in angularity. Based on these findings, it can be deduced that abrasion has the potential to change the surface roughness of coarse aggregates at the microscopic level. It is possible that the polishing of the aggregate surface that occurs during the abrasion process is responsible for the reduction in aggregate texture. Figure 7 plots the variance in texture distribution across the coarse aggregates. Figure 7 demonstrated that both before and after abrasion, a significant portion of the sample fell into the low and moderate texture categories with a proportion of roughly sixty percent or more. The mean value of texture for RAP experienced the most substantial decrease, with a 46% decrease. Only a small number of particulates in the most severe texture range were observed prior to the abrasion. This research suggests that the microscopic surface texture of coarse aggregates can be altered by abrasion. The abrasion process may have resulted in the aggregates

being polished, which could explain the subtle smoothing of the surface.

The sphericity percentage for four distinct aggregate types, both before and after they were subjected to abrasion, is shown in Figure 8. The Andesite aggregates' sphericity was seen to change most markedly after they were subjected to abrasion. The main cause of the minor increase in sphericity that was noticed was the rounding off coarse aggregates' sharp edges and corners. The disintegration of elongated or flat particles is another potential element in the formation of sphericity. The variance in the coarse aggregate's sphericity distribution and the shift in the sphericity mean value brought about by the abrasion test are shown in Figure 9. Of all the aggregate types, andesite aggregates saw the greatest increase in mean sphericity, rising by 18%. As shown in Fig. 9, all the aggregates that were in the moderate to high sphericity ranges rose into the high to extreme sphericity range after being subjected to abrasion. The reason for this could be that the round particles were harder to break than the flat or elongated ones.

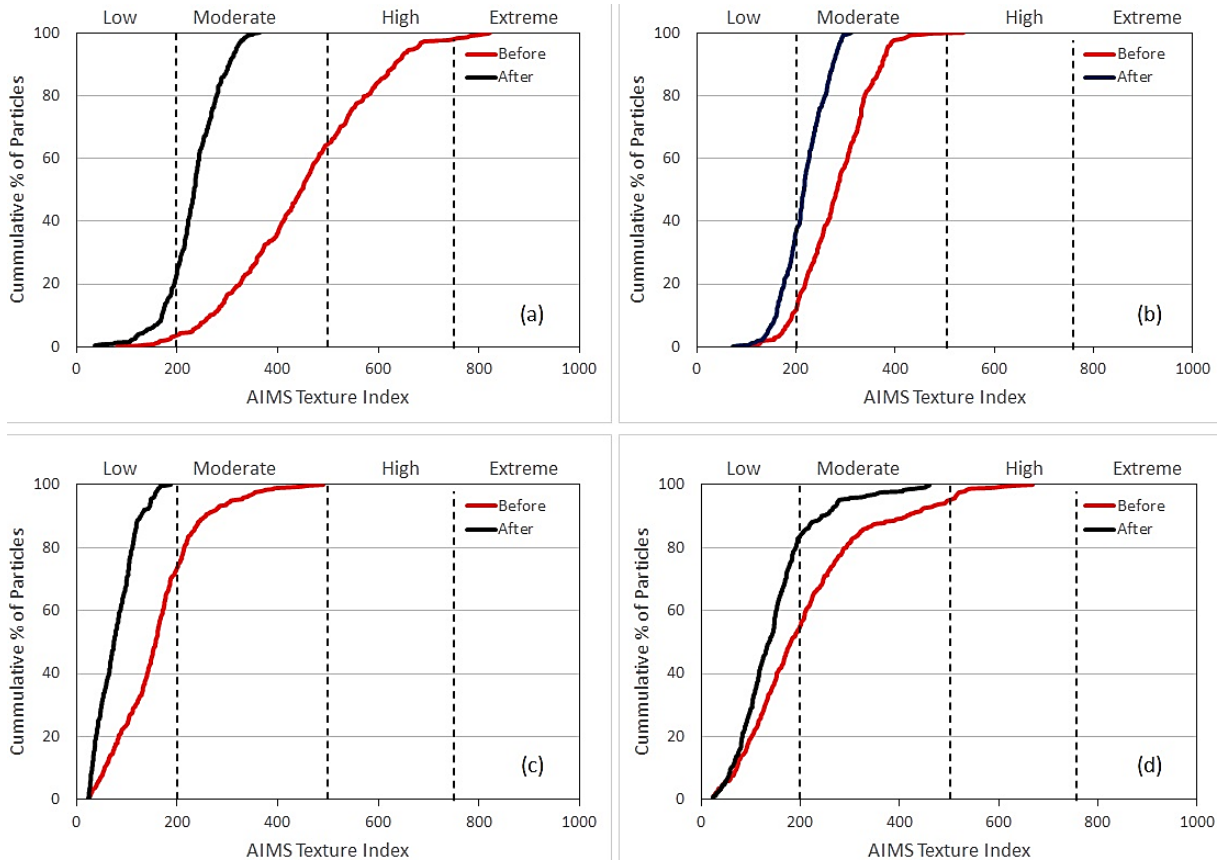


Figure 6. Surface Texture pre- and post-L.A. abrasion wear test (a) crushed Limestone (b) crushed Andesite (c) RAP (d) RCA

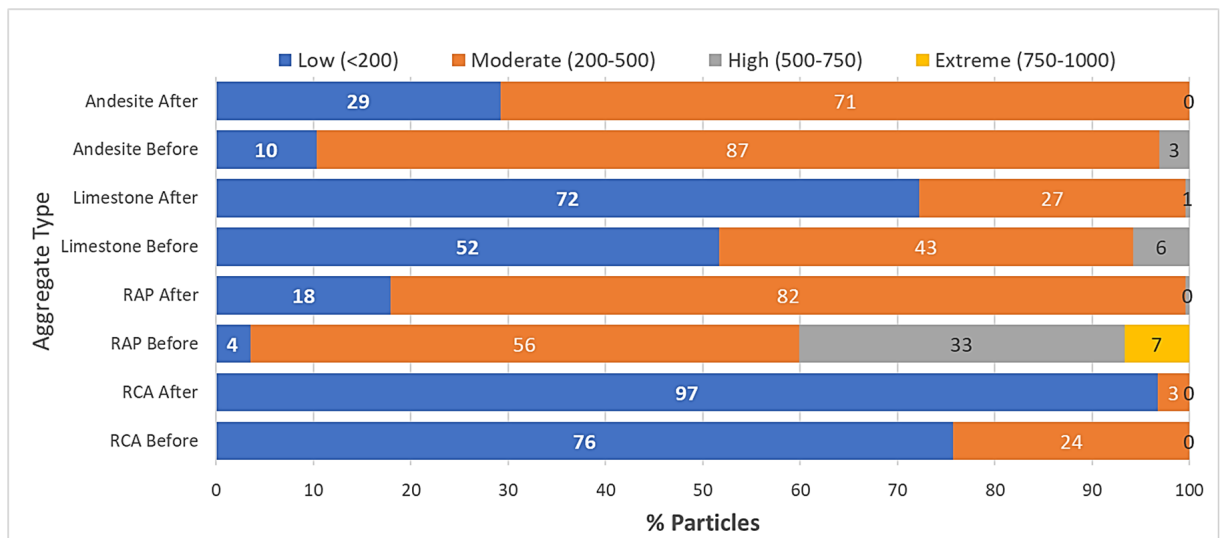


Figure 7. Angularity distribution of aggregates pre- and post-L.A. abrasion wear test

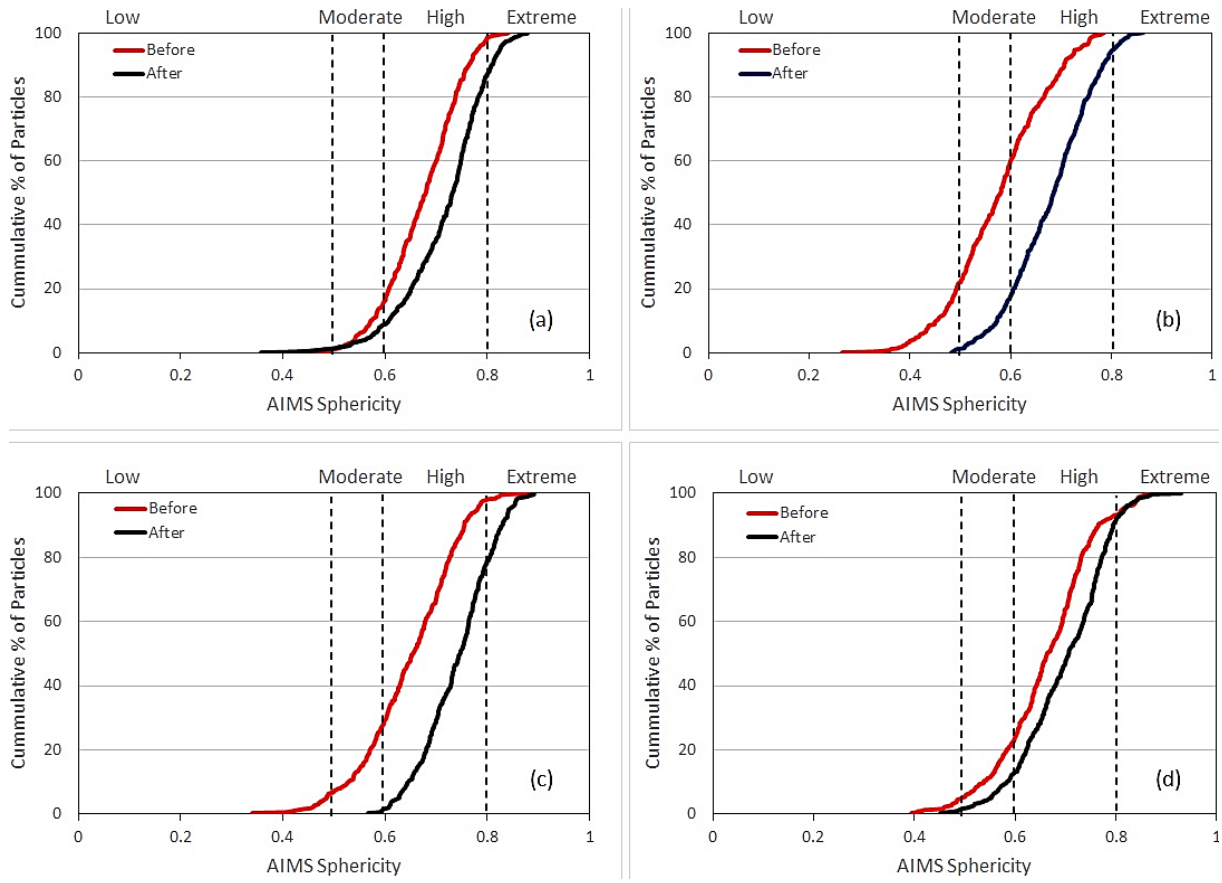


Figure 8. Sphericity pre- and post-LA abrasion wear test (a) crushed Limestone (b) crushed Andesite (c) RAP (d) RCA

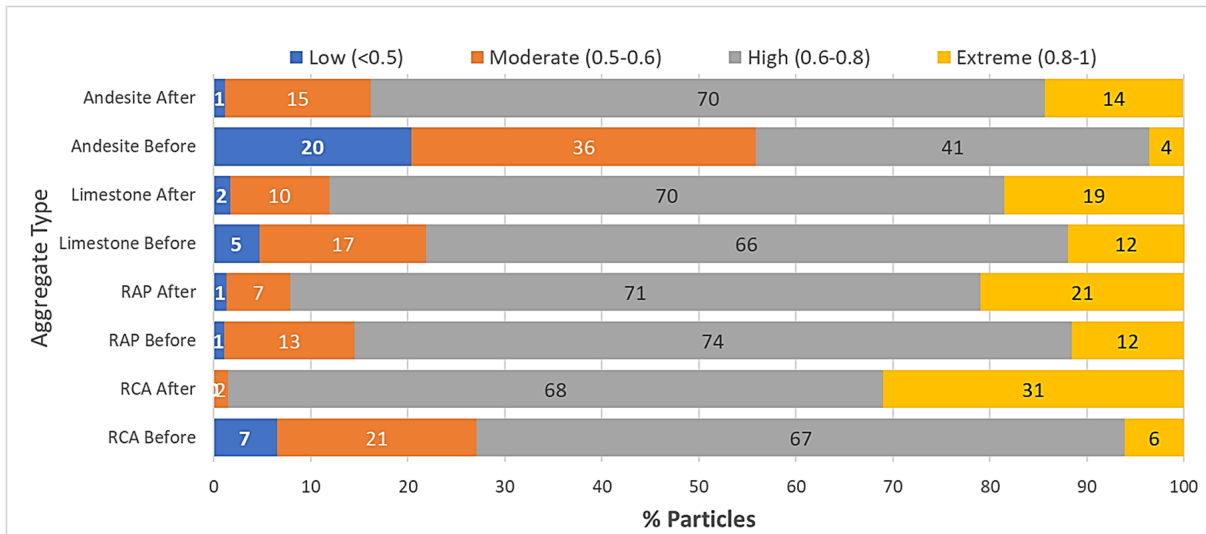


Figure 9. Sphericity distribution of aggregates pre- and post-L.A. abrasion wear test

3.3. Crack Displacement Curves and Patterns

The fracture patterns of the tested samples, as depicted in Figure 10, primarily move in a continuous upward trajectory from the notch to the region where the load was applied. The only exceptions to this pattern are the 0mm notch 40mm and 0mm notch 50mm GCS samples. These fracture patterns resemble those found in a prior study

conducted by [35] utilizing the SCB test on asphalt mixtures containing RAP. It was further observed that for the 40mm and 50mm GCS samples, it is seen that the samples that are notched 12.5 mm and 25 mm all have a consistent crack pattern while the crack patterns in the 0mm notch samples are mostly to one side of the sample. This identified that the presence of a notch in the GCS samples is the most effective as it initiates the behavior of

the crack better than the samples without. Additionally, the cracks are more visible in the notched samples with specimen thickness having no influence on the crack patterns as there were observed similarities when comparing the 40 mm RAP versus 50 mm RAP and the 40 mm GCS versus 50 mm GCS.

The maximal load of the samples is influenced by the notch depths, as evidenced by the load-displacement curves depicted in Figure 11. The peak load was found to decrease as the notch depth increased, as was the case in previous experiments conducted on comparable pavement materials [35, 36]. No significant difference in the peak loads was observed in the 40mm RAP versus the 50mm RAP samples. In the 40mm GCS versus the 50mm GCS samples, there is a major difference in the 0mm and 12.5mm samples as the peak loads are much larger in the 50mm GCS samples than the 40mm GCS samples. With an increase in thickness the sample has a much higher

peak load. This was also observed in the study by [37] who also showed that peak loads increase as specimens became thicker.

3.4. Peak Loads and Tensile Strength

Figure 12 highlights an increase in peak load with decrease in notch depth. This is consistent with the findings of [38], which evaluated the influence of notch length on asphalt samples. Tensile strength was observed to be greater in the 0 mm notch depth samples as expected as samples with lower notch depths require more energy to fracture because their areas are significantly bigger than samples with larger notch depths. Tensile strength values were observed to be greater in GCS samples than in RAP samples between ranges of 42 – 103% (Figure 13 and Table 2). The reference to the HMA mixture data is found in the research paper of [35].

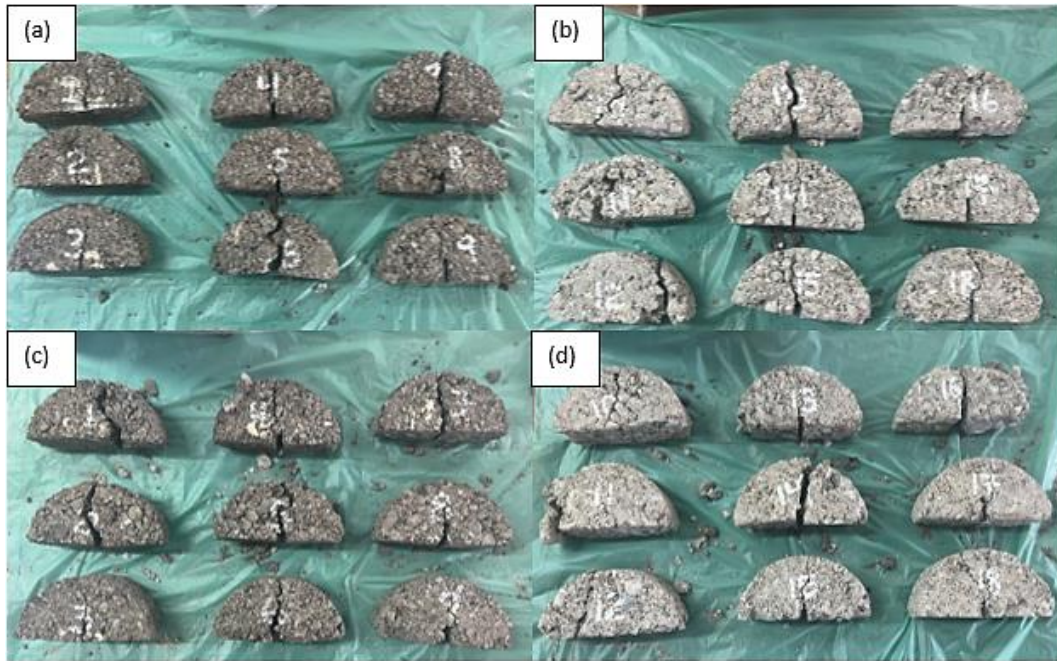


Figure 10. Cracks in BSM test specimens (a) 40mm-RAP (b) 40mm-GCS (c) 50mm-RAP (d) 50mm-GCS

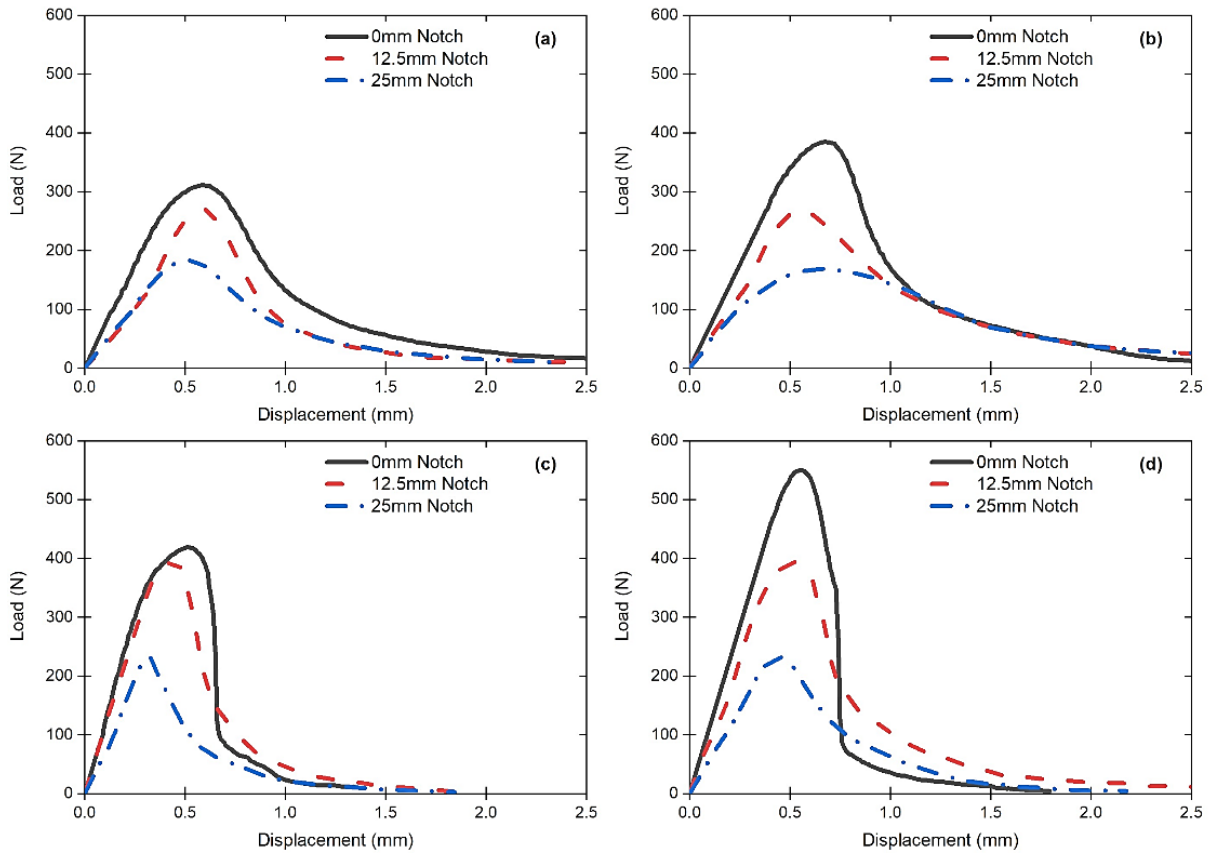


Figure 11. Load-displacement curves (a) 40mm RAP (b) 50mm RAP (c) 40mm GCS (d) 50mm GCS

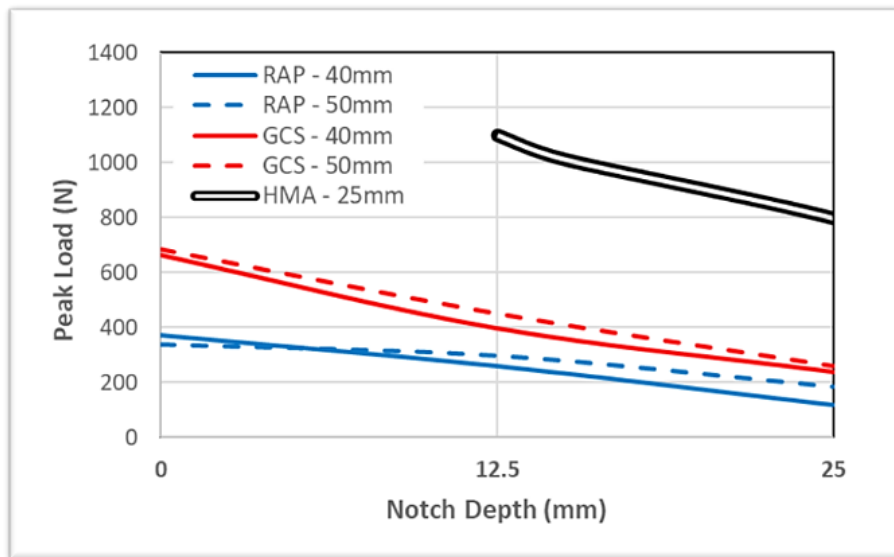


Figure 12. Peak load versus notch depth

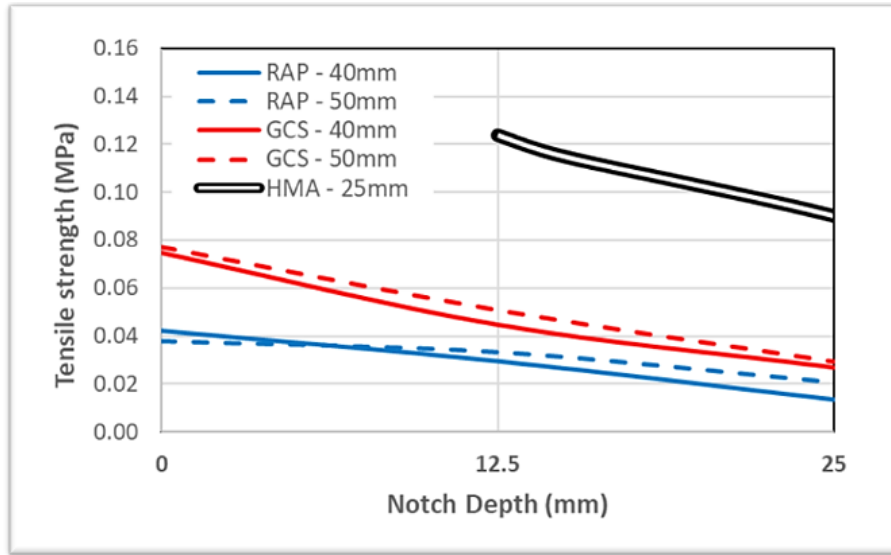


Figure 13. Tensile strength versus notch depth

Table 2. Summary of the peak load and tensile strength of BSM samples

BSM Material	Specimen Thickness (mm)	Notched Depth (mm)	Peak Load (N)				Tensile Strength (MPa)			
			min	avg	max	std. Dev.	min	avg	max	std. Dev.
RAP	40	0	310.8	373.1	431.0	60.2	0.04	0.04	0.05	0.01
	40	12.5	229.3	260.8	283.2	28.1	0.03	0.03	0.03	0.00
	40	25	94.3	118.7	142.5	24.1	0.01	0.01	0.02	0.00
	50	0	336.0	336.8	338.4	1.4	0.04	0.04	0.04	0.00
	50	12.5	245.0	295.5	373.2	68.3	0.03	0.03	0.04	0.01
	50	25	161.8	182.6	216.8	29.8	0.02	0.02	0.02	0.00
GCS	40	0	575.3	662.4	721.0	77.0	0.07	0.07	0.08	0.01
	40	12.5	392.4	397.0	403.5	5.8	0.04	0.04	0.05	0.00
	40	25	231.8	239.2	248.3	8.4	0.03	0.03	0.03	0.00
	50	0	595.5	683.5	802.0	106.6	0.07	0.08	0.09	0.01
	50	12.5	200.0	449.9	634.5	224.5	0.02	0.05	0.07	0.03
	50	25	212.5	259.1	332.4	64.2	0.02	0.03	0.04	0.01
% Difference between RAP and GCS	40	0	78%				78%			
	40	12.5	52%				52%			
	40	25	102%				102%			
	50	0	103%				103%			
	50	12.5	52%				52%			
	50	25	42%				42%			

3.5. Fracture Energy

As identified in Figure 14, for the 40mm GCS, 50mm RAP and GCS samples, an increase in notch depth is accompanied with a decrease in fracture energy. However, in the 40mm RAP samples, the fracture energy increases, then decreases, but the values are very close to each other. Consistent with a study by [37], a diminishing trend in fracture energy was noted with an increase in notch length; it was shown that the energy absorbed diminishes as the

ligament area of the sample decreases. Upon comparison of thickness, it is seen that the fracture energy in the 40mm GCS samples exceeds that of the 50mm GCS samples. Nevertheless, it is elevated in the 50mm RAP samples compared to the 40mm RAP samples (Table 3). This is in accordance with findings of SCB testing on asphaltic concrete by [39]. The fracture energy increased from 30 mm to 50 mm, and then slightly decreased at a thickness of 60 mm, according to the findings of this study.

3.6. Fracture Toughness

As identified in Figure 15, the fracture toughness in the 50mm RA P, 40mm GCS and 50mm GCS increases as the notch depth increases. The toughness increases with the

12.5mm notch and then decreases with the 25mm notch. The fracture toughness was observed to be higher in the 40mm GCS samples than the 50mm GCS samples (Table 3). It is higher in the 50mm RAP samples than the 40mm RAP samples.

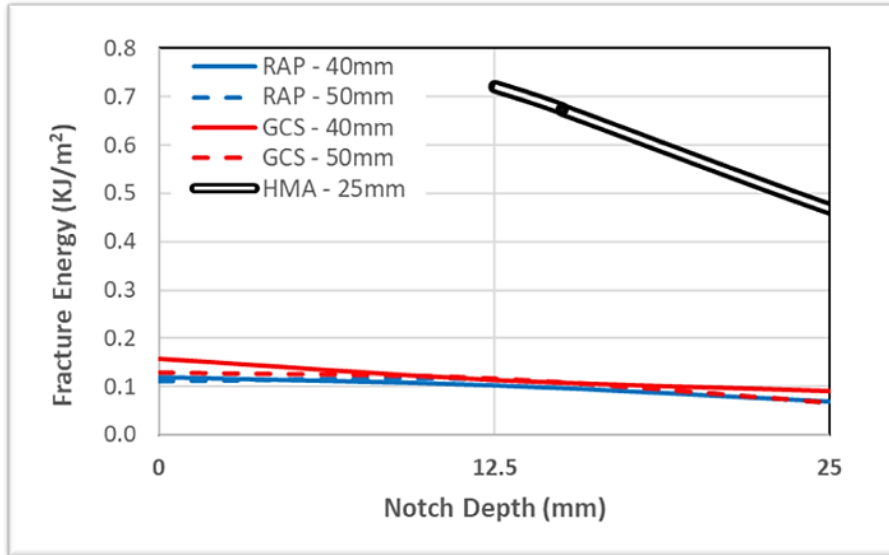


Figure 14. Fracture energy vs. notch depth

Table 3. Summary of the fracture energy and fracture toughness of BSM samples

BSM Material	Specimen Thickness (mm)	Notched Depth (mm)	Fracture Energy (KJ/m ²)				Fracture Toughness (MPa.m ^{1/2})			
			min	avg	max	std. Dev.	min	avg	max	std. Dev.
RAP	40	0	0.10	0.12	0.13	0.02				
	40	12.5	0.06	0.10	0.17	0.06	20.9	24.2	26.2	2.8
	40	25	0.03	0.07	0.12	0.04	14.3	18.4	22.5	4.1
	50	0	0.11	0.11	0.11	0.00				
	50	12.5	0.06	0.11	0.14	0.04	17.2	21.1	27.3	5.4
	50	25	0.00	0.07	0.11	0.06	0.1	15.3	26.4	13.6
GCS	40	0	0.15	0.16	0.17	0.01				
	40	12.5	0.06	0.11	0.20	0.08	34.7	35.5	36.6	0.9
	40	25	0.05	0.09	0.16	0.06	33.9	35.6	37.7	1.9
	50	0	0.05	0.13	0.17	0.07				
	50	12.5	0.08	0.12	0.16	0.04	13.1	31.6	44.5	16.4
	50	25	0.05	0.07	0.09	0.02	26.5	30.8	38.5	6.7
% Difference between RAP and GCS	40	0	32%				-			
	40	12.5	11%				47%			
	40	25	31%				94%			
	50	0	16%				-			
	50	12.5	3%				49%			
	50	25	3%				101%			

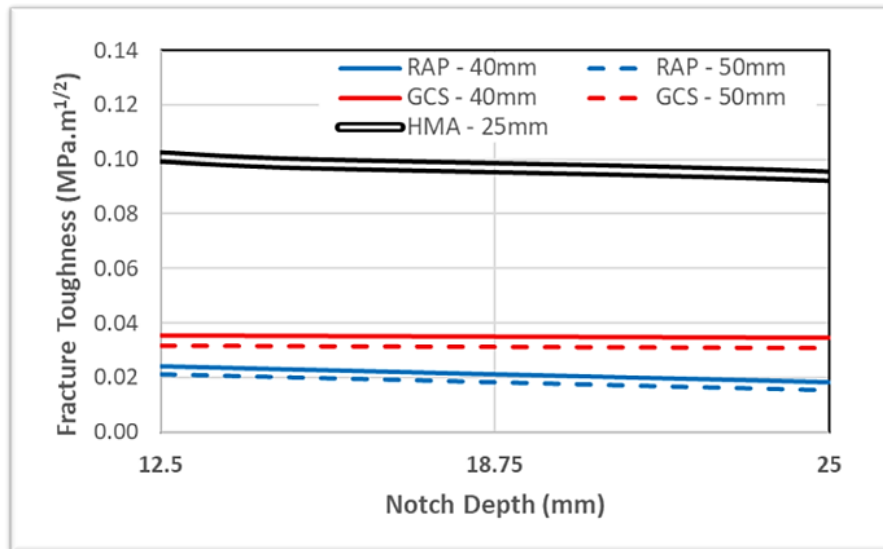


Figure 15. Fracture toughness vs. notch depth

4. Conclusions

In this work, coarse aggregates in-service were subjected to simulated abrasion applied by vehicle wheel loading using the Los Angeles abrasion test. Additionally, the influence of attrition on the morphologies of various coarse aggregates was under investigation. Limestone, andesite, recycled concrete aggregate and recycled asphalt pavements were as the coarse aggregates of choice. The morphological properties of a variety of coarse aggregates were put through an abrasion test and then quantified and studied before and after the test. The following conclusions can be derived from the study:

- 1) The abrasion resistance of coarse aggregates is influenced by the diverse mineral and physical components that make up the aggregate. RCA aggregates have the lowest resistance to abrasion during the abrasion process, followed by limestone, RAP, and andesite. The observed durability and capability of the andesite aggregate to endure the impact of traffic loads are demonstrated by the low abrasion wear it experiences.
- 2) Although RAP aggregates showed the highest angularity decline, followed by RCA, limestone, and andesite, identifying angularity reduction as a major component of abrasion loss, their abrasion values were not consistent. The abrasion test has the potential to influence the microscopic surface texture of coarse aggregates, as evidenced by the significant variation in coarse aggregate surface texture before and after abrasion, similar to angularity. Therefore, for pavements with strong anti-skid requirements, coarse aggregates with a high angularity and a low abrasion value should be taken into consideration.
- 3) The lowering of angularity is the main cause of abrasion loss; the smoothing of coarse aggregate edges and borders drastically changes the sphericity.

Utilizing previous testing variables used in SCB testing on asphalt mixtures (i.e., thickness and notch length), Bitumen stabilized material samples were tested to determine the SCB test as a suitable test. Based on the test-analysis conducted on the data from the SCB test, the following conclusions can be drawn:

- 1) The thickness of the sample does not have any influence on the crack pattern for the 40mm RAP vs. 50mm RAP and the 40mm GCS vs. 50mm GCS. Notching the GCS samples is effective as it produces a better crack pattern. Notched specimens from RAP and GCS materials exhibit superior crack patterns compared to their counterparts with 0mm notches. Identical crack patterns were noted in both the RAP and GCS notched specimens, with cracking commencing at the notched extremity and progressing vertically. In 0 mm notched specimens, cracking in the GCS specimens was noted to initiate around the support (roller) location of the test apparatus. Nonetheless, the fracture originated at the center of the 0 mm notched RAP-BSM specimens. The elasticity of the RAP sample may have influenced this behavior in contrast to the more rigid behavior of a GCS-BSM material.
- 2) Notching the samples has an influence on the peak load of the samples as increasing the notch depth decreases the peak load. In terms of thickness there is no major difference in the 40mm and 50mm RAP samples, as the peak loads are generally approximately the same with the thicker sample being slightly higher. The 40mm and 50mm GCS samples displayed a trend that with an increase in thickness the sample has a much higher peak load. Therefore, as the samples thickness increased, the peak load increased.
- 3) The tensile strength is higher in the 0mm notch depth samples compared to the 12.5mm and 25mm notched samples. The tensile strength is also higher

in the 50mm GCS and RAP samples compared to the 40mm GCS and RAP samples. Notch depth and thickness do have an influence on tensile strength in the samples. As the notch increased, the tensile strength decreased in all samples.

- 4) The fracture energy is influenced by the notch depth and thickness for all samples. As the notch depth increased, the fracture energy decreased. As thickness increased in the RAP samples, fracture energy increased but as thickness increased in the GCS samples, fracture energy decreased.
- 5) The fracture toughness is influenced by the notch depths and thickness. It decreases as notched depths increase in all samples. The fracture toughness is lower in the thicker (50mm) GCS samples and (50mm) RAP samples.

Based on these conclusions, it is recommended to use a minimum of 6 samples when performing the SCB test to improve accuracy of measure. Additionally, it is recommended that further studies be carried out using thicker specimens to investigate the influence on SCB test behavior, fracture energy and fracture toughness. In conclusion, the Semi-Circular Bend test method was shown to be a reliable and appropriate test method for evaluating the fracture behavior of Bitumen Stabilized Materials.

Acknowledgements

For their cooperation in the implementation of the mix design and tests, the authors would like to express their gratitude to all of the technicians who worked in the Highway and Transportation Laboratory at the Department of Civil and Environmental Engineering, located on the St. Augustine Campus of the University of the West Indies (UWI) and Beyond Engineering Ltd. The natural and recycled concrete aggregates were supplied by local contractors, and the authors would like to publicly acknowledge their contributions.

REFERENCES

- [1] Meddage D. P. P., Chadee A., Jayasinghe M. T. R., Rathnayake U., "Exploring the applicability of expanded polystyrene (EPS) based concrete panels as roof slab insulation in the tropics," *Case Studies in Construction Materials*, vol. 17, 2022. DOI: 10.1016/j.cscm.2022.e01361
- [2] Fu P., "Micromechanics for Foamed Asphalt Stabilised Materials," Ph.D. Dissertation. University of California, Davis, USA, 2009.
- [3] Maerz N., "Technical and computational aspects of the measurement of aggregate shape by digital image analysis," *Journal of Computing in Civil Engineering*, vol. 18, no. 1, pp. 10–18, 2004. DOI: 10.1061/(ASCE)0887-3801(2004)18:1(10)
- [4] Wang H., Wang D., Liu P., Hu J., Schulze C., Oeser M., "Development of morphological properties of road surfacing aggregates during the polishing process," *International Journal of Pavement Engineering*, vol. 18, no. 4, pp. 367–380, 2017. DOI: 10.1080/10298436.2015.1088153
- [5] Barksdale R. D., Itani S. Y., "Influence of Aggregate Shape on Base Behavior," *Transportation Research Record*, no. 1227, pp. 173–182, 1989.
- [6] Chen J. S., Chang M. K., Lin K. Y., "Influence of coarse aggregate shape on the strength of asphalt concrete mixtures," *Journal of the Eastern Asia Society for Transportation Studies*, vol. 6, pp. 1062-1075, 2005. DOI: 10.11175/easts.6.1062
- [7] Masad E., Fletcher T., "Aggregate imaging system (AIMS): Basics and applications," Texas Transportation Institute, Texas A&M University System, No. FHAWA/TX-05/5-17 07-01-1, 2005.
- [8] Sabita, South African Bitumen Association. "Technical Guideline: Bitumen Stabilised Material: A Guideline for the Design and Construction of Bitumen Emulsion and Foamed Bitumen Stabilised Materials, TG2 3rd Edition." 1–221. ISBN 978-1-874968-77-1. Pretoria, South Africa, 2020.
- [9] Jenkins K., "Cracking Behaviour of Bitumen Stabilised Materials (BSMs): Is There Such a Thing?," RILEM International Conference on Cracking in Pavements, RILEM Bookseries, vol 4., 2012.
- [10] Teixeira J. E. S. L., Junior C. M. A., de Rezende L. R., Branco V. T. F. C., Kim Y. R., "Evaluation of asphalt concrete's fatigue behavior using cyclic semi-circular bending test," *Construction and Building Materials*, no. 400, pp. 132772, 2023. DOI: 10.1016/j.conbuildmat.2023.132772
- [11] Elseifi M. A., "Modeling and evaluation of the cracking resistance of asphalt mixtures using the semi-circular bending test at intermediate temperatures," *Road Material and Pavement Design*, no. 13, pp. 124–139, 2012. DOI: 10.1080/14680629.2012.657035
- [12] Ozer H., Al-Qadi I. L., Lambros J., El-Khatib A., Singhvi P., Doll B., "Development of the fracture-based flexibility index for asphalt concrete cracking potential using modified semi-circle bending test parameters," *Construction and Building Materials*, vol. 115, pp. 390–401, 2016. DOI: 10.1016/j.conbuildmat.2016.03.144
- [13] Xu D., Ni F., Du H., Zhao Z., Wang J., Chen S., "Investigation of Factors Affecting the Intermediate-Temperature Cracking Resistance of In-Situ Asphalt Mixtures Based on Semi-Circular Bending Test," *Coatings*, vol. 13, no. 2, pp. 384, 2023. DOI: 0.3390/coatings13020384
- [14] Safazadeh F., Romero P., Mohammad Asib A. S., VanFrank K., "Methods to evaluate intermediate temperature properties of asphalt mixtures by the semi-circular bending (SCB) test," *Road Materials and Pavement Design*, vol. 23, no. 7, pp.1694-1706, 2022. DOI: 10.1080/14680629.2021.1911831
- [15] Bui H. H., Saleh M., "Effects of specimen size and loading conditions on the fracture behaviour of asphalt concretes in

- the SCB test.” *Engineering Fracture Mechanics*, vol. 242, pp. 107452, 2021. DOI: 10.1016/j.engfracmech.2020.107452
- [16] Nsengiyumva G., Kim Y. R., “Effect of testing configuration in semi-circular bending fracture of asphalt mixtures: experiments and statistical analyses,” *Transportation Research Record*, vol. 2673, no. 5, pp. 320-328, 2019. DOI: 10.1177/0361198119839343
- [17] Saha G., Biligiri K. P., “Fracture properties of asphalt mixtures using semi-circular bending test: a state-of-the-art review and future research,” *Construction and Building Materials*, vol. 105, pp. 103-112, 2016. DOI: 10.1016/j.conbuildmat.2015.12.046
- [18] Masad E., “The Development of a Computer Controlled Image Analysis System for Measuring Aggregate Shape Properties,” Report No. NCHRP-IDEA Project 77, Transportation Research Board of the National Academy, Washington, DC, USA, 2003.
- [19] Masad E., Al-Rousan T., Button J., Little D., Tutumluer E., “Test Methods for Characterizing Aggregate Shape, Texture, and Angularity,” NCHRP Rep. No. 555, Transportation Research Board of the National Academy, Washington, DC, USA, 2007.
- [20] Fletcher T., Chandan C., Masad E., Sivakumar K., “Aggregate imaging system for characterizing the shape of fine and coarse aggregates,” *Transportation Research Record*, no. 21832, pp. 67–77, 2003. DOI: 10.3141/1832-09
- [21] ASTM. “ASTM C802-96 Standard Practice for Conducting an Interlaboratory Test Program to Determine the Precision of Test Methods for Construction Materials,” American Society for Testing and Materials) International, West Conshohocken, PA, USA, 1996a.
- [22] ASTM. “ASTM C1067-96 Standard Practice for Conducting a Ruggedness or Screening Program for Test Methods for Construction Materials,” American Society for Testing and Materials) International, West Conshohocken, PA, USA, 1996b.
- [23] ASTM. “ASTM C131-21 Standard Test Method for Resistance to Degradation of Small-Size Coarse Aggregate by Abrasion and Impact in the Los Angeles Machine,” American Society for Testing and Materials) International, West Conshohocken, PA, USA, 2021.
- [24] AASHTO. “AASHTO TP 105-13 Standard Method of Test for Determining the Fracture Energy of Asphalt Mixtures Using the Semi-Circular Bend Geometry (SCB),” American Association of State Highway and Transportation Officials, Washington, DC, USA, 2013.
- [25] AASHTO. “AASHTO TP 124-16 Standard Method of Test for Determining the Fracture Potential of Asphalt Mixtures Using the Flexibility Index Test (FIT),” American Association of State Highway and Transportation Officials, Washington, DC, USA, 2016.
- [26] Saed S. A., Kamboozia N., Ziari H., Hofko B., “Experimental assessment and modeling of fracture and fatigue resistance of aged stone matrix asphalt (SMA) mixtures containing RAP materials and warm-mix additive using ANFIS method,” *Materials and Structures*, vol. 54, no. 225, 2021. DOI: 10.1617/s11527-021-01812-9
- [27] Mansourian A., Razmi A., Razavi M., “Evaluation of fracture resistance of warm mix asphalt containing jute fibers,” *Construction and Building Materials*, vol. 117, pp. 37–46, 2016. DOI: 10.1016/j.conbuildmat.2016.04.128
- [28] Anderson T.L., “Fracture mechanics: fundamentals and applications,” CRC press, 2005.
- [29] Faraj R. H., Aryan F. H. S., “Handbook of Sustainable Concrete and Industrial Waste Management,” Woodhead Publishing, 2022.
- [30] Vaidya A., Pathak K., “Mechanical stability of dental materials,” *Applications of Nanocomposite Materials in Dentistry*, vol. 17, pp. 285–305, 2019. DOI: 10.1016/B978-0-12-813742-0.00017-1
- [31] Zhou F., Im S., Sun L., Scullion T., “Development of an IDEAL Cracking Test for Asphalt Mix Design and QC/QA,” *Road Material and Pavement Design*, vol. 18, pp. 405–427, 2017. DOI: 10.1080/14680629.2017.1389082
- [32] Molenaar J. M. M., “Performance Related Characterisation of the Mechanical Behavior of Asphalt Mixtures,” Ph.D. Thesis, Delft University of Technology, Delft, The Netherlands, 2003.
- [33] Jiang J., Dong Q., Ni F., Zhao Y. J., “Effects of Loading Rate and Temperature on Cracking Resistance Characteristics of Asphalt Mixtures Using Non-Notched Semi-circular Bending Tests,” *Journal of Testing and Evaluation*, vol. 47, no. 4, 2019. DOI: 10.1520/JTE20170711
- [34] Mahmoud E., Ortiz E., “Implementation of AIMS in Measuring Aggregate Resistance to Polishing, Abrasion, and Breakage,” FHWA-ICT-14-014 (2014), Illinois Center for Transportation, Department of Civil and Environmental Engineering, University of Illinois University at Urbana-Champaign: Springfield, IL, USA, 2014.
- [35] Leon L., Smith J., Frank A., “Intermediate Temperature Fracture Resistance of Stone Matrix Asphalt Containing Untreated Recycled Concrete Aggregate,” *The Baltic Journal of Road and Bridge Engineering*, vol. 18, no. 1, pp. 94-121, 2023. DOI: 10.7250/bjrbe.2023-18.590
- [36] Lu D. X., Saleh M., Nguyen N. H., “Evaluation of fracture and fatigue cracking characterization ability of non-standardized semi-circular-bending test for asphalt concrete,” *Journal of Materials in Civil Engineering*, vol. 32, no. 8, pp. 04020215, 2020. DOI: 10.1061/(ASCE)MT.1943-5533.0003292
- [37] Nsengiyumva G., Kim Y-R., You T., “Development of a Semicircular Bend (SCB) Test Method for Performance Testing of Nebraska Asphalt Mixtures,” Nebraska Department of Roads Research, Reports 171, 2015.
- [38] Nsengiyumva G., You T., Kim Y-R., “Experimental-Statistical Investigation of Testing Variables of a Semicircular Bending (SCB) Fracture Test Repeatability for Bituminous Mixtures,” *Journal of Testing and Evaluation*, vol. 45, no. 5, pp. 691-1701, 2017.
- [39] Nsengiyumva G., “Development of Semi-Circular Bending (SCB) Fracture Test for Bituminous Mixtures,” MS.C. Thesis. The Graduate College at the University of Nebraska, USA, 2015